JGR Earth Surface

RESEARCH ARTICLE
10.1029/2020JF005584

Effect of Small Tidal Fluctuations on the Stability and Equilibrium Configurations of Bifurcations

Niccolò Ragno[1], Nicoletta Tambroni[1], and Michele Bolla Pittaluga[1]

[1]Department of Civil, Chemical and Environmental Engineering, University of Genoa, Genoa, Italy

Deltas are fascinating landforms subject to fluvial and marine forcing. Bifurcations are common features in deltas, governing the distribution of water and sediment fluxes among the distributary channel network. Recently, it has been observed that tide-influenced deltas tend to display less numerous but more stable branches in comparison to their riverine counterparts. River bifurcations subject to unidirectional flow have been widely studied in the last decades. In contrast, the acting physical mechanisms and factors controlling the stability of bifurcations in tide-influenced deltas are still not well understood, and a theoretical framework is still lacking. In order to fill this gap and understand how the stability and evolution of bifurcations in distributary deltaic systems could be affected by the tides, we investigate, through an analytical model, the equilibrium configurations and stability of tidal bifurcations under the hypothesis of small monochromatic tidal oscillations. In particular, we build on previous works on river bifurcations, incorporating the solution for the equilibrium of a single-river-dominated estuary. We find that higher tidal amplitudes and a closer proximity of the junction node to the sea tend to hamper the development of unbalanced solutions, reducing the asymmetries in water and sediment fluxes between branches. This stabilizing effect exerted by the tidal action is associated with the erosive character of the tidal currents that promotes channel deepening and increases the capacity of the system to keep morphodynamically active both bifurcates in comparison with the purely fluvial case. Preliminary field observations of natural deltas corroborate our findings.

Key Points:
- Tidal amplitude and bifurcate length are key control parameters of tidal bifurcations
- Higher tidal amplitudes and shorter lengths tend to reduce the inequalities in sediment and discharge partition
- Micro-tidal bifurcations are more likely to keep both downstream branches morphodynamically active compared to their fluvial counterparts

Supporting Information:
- Supporting Information S1

Correspondence to:
N. Ragno,
niccolo.ragno@edu.unige.it

Citation:
Ragno, N., Tambroni, N., & Bolla Pittaluga, M. (2020). Effect of small tidal fluctuations on the stability and equilibrium configurations of bifurcations. *Journal of Geophysical Research: Earth Surface*, *125*, e2020JF005584. https://doi.org/10.1029/2020JF005584

Received 20 FEB 2020
Accepted 22 JUL 2020
Accepted article online 28 JUL 2020

1. Introduction

Deltas are low-lying landscapes shaped from the dynamic interaction of fluvial (input of water and sediment) and marine processes (waves and tides). The complex interactions between these mechanisms determine the morphodynamic evolution, typically creating a network of branches unraveling from a delta apex. In this context, from a reductionist point of view, single bifurcations of the delta represent the building blocks, controlling the distribution of water, sediment, and nutrient fluxes among the branches. Understanding their dynamics is therefore important in an era of climate changes and anthropogenic pressure on coastal areas that makes deltas vulnerable elements, threatened by degradation due to extraction of natural resources (oil and gases, and sand mining), land reclamation, sediment retention by reservoirs, and harbors development (Hackney et al., 2020; Hoitink et al., 2017, 2020).

The imprint of tides appears in real-world tidally influenced deltas as shown in Figure 1. These landforms can show a range of scales (Sassi et al., 2012), with upper regions characterized by fairly prismatic non-converging reaches (river-dominated reach), and by sinuous, funnel-shaped estuarine channels in the seaward portions of the delta, often disconnected from the main distributaries (tide-dominated reach) (Figures 1a and 1b). In the case of a micro-tidal delta like the Wax Lake Delta (Figure 1c) branches are more symmetric and characterized by a fairly constant width while approaching the sea. While the Wax Lake Delta represents a model for the study of delta restoration projects to counteract wetland degradation (Hiatt & Passalacqua, 2015; Paola et al., 2011), human-based engineering interventions in deltas are common as fluvial navigation is a fundamental economic resource worldwide, as in the case of Yangtze River (Figure 1d). A common practice in these cases is the deepening of one channel to facilitate ships navigation. This however has important implications for the evolution of the whole system, since it affects the equilibrium of branches, possibly leading to channels infilling and sediment accumulation as reported in the Yangtze River Delta (Zhang et al., 2019).

In the last decades, several analytical, numerical, and experimental works have been carried out to firstly investigate the equilibrium and stability of fluvial bifurcations (e.g., Bolla Pittaluga, Coco, & Kleinhans,

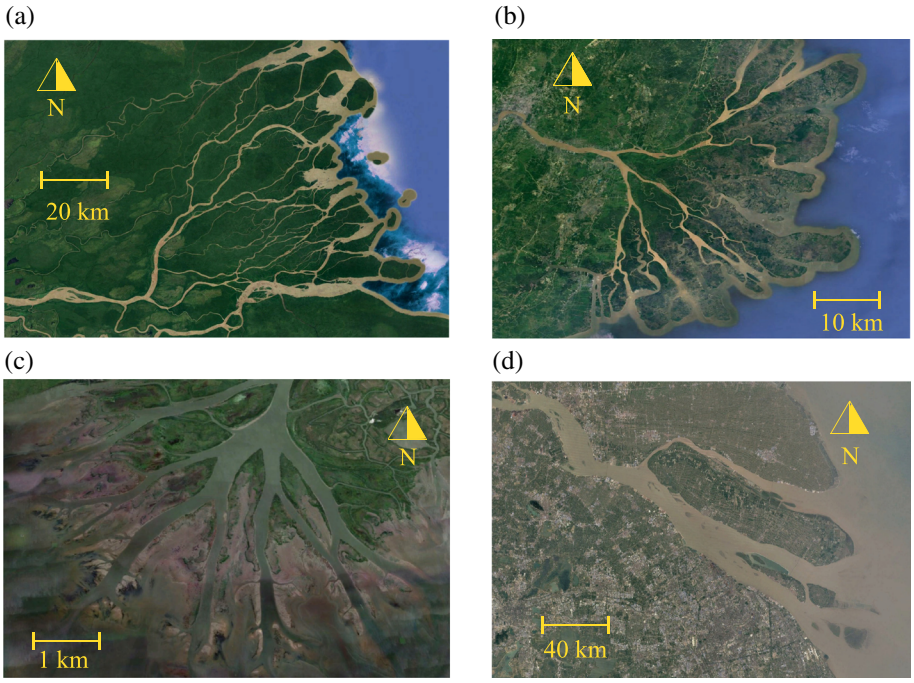

Figure 1. Satellite images of natural deltas: (a) delta of Orinoco River (Venezuela), 8°49′N, 61°04′W, and (b) Mahakam Delta (Indonesia), 0°35′S, 117°17′W, both deltas of the equatorial zone; the separation between a region dominated by the river, and a region dominated by the tide, exhibits itself through a clear break in geometric properties of the channels; (c) Wax Lake Delta (USA), 29°32′N, 91°25′W, a typical example of a micro-tidal delta characterized by a fairly symmetric channel network; (d) delta of Yangtze River (China), 31°42′N, 121°11′E, characterized by a strong asymmetry at the bifurcation near the delta apex, the narrower channel has undergone to progressive infilling during the last century. From *Google Earth, Digital Globe (2019)*.

2015; Bolla Pittaluga et al., 2003; Edmonds & Slingerland, 2008; Wang et al., 1995) and then to include the role of different upstream boundary conditions, such as the presence of migrating bars or meander bends, in controlling the route of water and sediment fluxes in the downstream branches (e.g., Bertoldi et al., 2009; Kleinhans et al., 2008; Redolfi et al., 2019; Salter et al., 2018).

Recently, Salter et al. (2018) highlighted the important role exerted by the downstream boundary conditions, in determining the bifurcation dynamics in river-dominated deltas. In their study, the depositional fraction of the incoming splitting sediment (expressed through a differential relation) and the downstream channels length emerge as key factors in determining the morphological evolution of the system.

Additionally, numerical and field-case studies have revealed that even small-amplitude tides can strongly affect the hydrodynamics and morphology of micro-tidal deltas, and indeed, the water and sediment discharge distribution at channel junctions (e.g., Buschman et al., 2010; Iwantoro et al., 2019; Sassi et al., 2011; Wagner & Mohrig, 2019). In a more holistic approach, results from physics-based morphodynamic simulations and laboratory experiments (e.g., Lentsch et al., 2018; Rossi et al., 2016) have shown how the mobility of the channels decreases with increasing of the tidal energy, due to an enhanced ability of tidal currents to flushing away bed material sediment. Tidal action then prevents aggradation through backfilling, a process considered to be one of the main triggering mechanisms for channel avulsion (Hoitink et al., 2020; Slingerland & Smith, 2004).

In the present contribution we deal with the equilibrium configurations and stability of a river bifurcation subject to a small tidal forcing (i.e., when the magnitude of the tidal amplitude is much smaller than water depth). This is achieved through the development of a one-dimensional model, building on the previous works of Bolla Pittaluga, Coco, and Kleinhans (2015) and Seminara et al. (2012) relative to the equilibrium and stability of a single bifurcation, and to the long-term equilibrium of a single-river-dominated estuary, respectively.

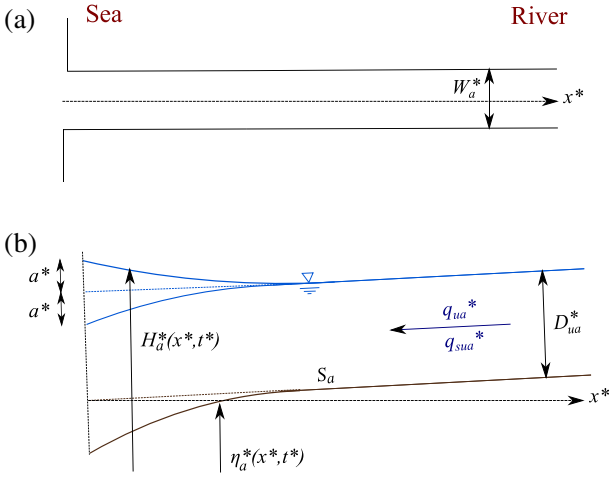

Figure 2. Representation of the (a) plan view and (b) longitudinal section of a tidal estuary, with notations.

We briefly provide an overview of these two main studies in section 2 and then formulate the one-dimensional model in section 3. In section 4 the problem is firstly linearized to understand which are the key controlling parameters affecting the behavior of the system, and then, the fully nonlinear system is solved numerically. The main implications of the results are discussed in section 5, while section 6 is devoted to some concluding remarks.

2. Equilibrium of Tidal Estuaries and River Bifurcations

2.1. Morphodynamic Equilibrium of Tidal Estuaries

The formal existence and definition of the morphodynamic equilibrium of an alluvial estuary has been a discussed topic, where the proper choice of a temporal and spatial scale is crucial (Zhou et al., 2016). Some initial approach to the problem consisted in neglecting the contribution of river discharge, referring to the limit case of tidal channels with typical converging shape found in coastal lagoons or in the tide-dominated parts of deltas (Kästner et al., 2017; Sassi et al., 2012). This case of single tidal channel has been investigated theoretically (e.g., Schuttelaars & Swart, 2000; Seminara et al., 2010), numerically (Lanzoni & Seminara, 2002; Todeschini et al., 2008; Xu et al., 2019), and in physical laboratory experiments (Kleinhans et al., 2014; Tambroni et al., 2005). Recently, Seminara et al. (2012) and Bolla Pittaluga, Tambroni, et al. (2015) tackled analytically and numerically the more general case of natural streams in which both river and tides concur. This case has been also subject to a series of laboratory and numerical investigations in a single channel (Leuven et al., 2018) and in a built-up physical tide-influenced delta (Finotello et al., 2019; Lentsch et al., 2018; Rossi et al., 2016).

The concept of morphodynamic equilibrium for an alluvial river is defined as the condition at which neither erosion nor deposition pattern variations can be observed at any cross section. In the one-dimensional framework here adopted, the above condition implies that the instantaneous longitudinal sediment flux must be constant throughout the channel and equal to the constant sediment flux delivered by the river (Bolla Pittaluga, Tambroni, et al., 2015):

$$\frac{\partial \eta^*(x^*,\, t^*)}{\partial t^*} = 0 \rightarrow q_s^* = \text{constant}, \tag{1}$$

where η^* denotes the bed elevation, t^* is time, x^* the spatial longitudinal coordinate, and q_s^* the longitudinal sediment flux per unit width. From hereinafter the star apex denotes dimensional quantities.

In the case of channels affected by both river and tidal forcing, following the approach of Seminara et al. (2012), a weaker form of equilibrium, defined as tidally averaged morphodynamic equilibrium, is achieved when the bed elevation does not experience any net variation in a tidal cycle (Bolla Pittaluga, Tambroni, et al., 2015):

$$\eta^*(x^*)\big|_{t^*}^{t^*+T^*} = 0, \tag{2}$$

with T^* tidal period.

Equation 2 does not account for phenomena like soil subsidence and sea-level rise that may affect the long-term equilibrium. In that case, a more general form of Equation 2 would require that the bed elevation relative to the mean sea level at a given time does not experience a net variation in a tidal cycle. Despite the fact that in nature tide oscillations and river discharge are intrinsically unsteady, the above condition provides a reference asymptotic state of conceptual relevance.

Let us now recall the main features of the model of Seminara et al. (2012) in the case of a constant width estuary, which will be later employed in the present formulation. The considered geometry and notation are sketched in Figure 2. More in detail, we refer to an estuary a with a rectangular cross section of

constant width W_a^*. Following the approach of Seminara et al. (2012), let us denote by x^* a longitudinal coordinate pointing landward with origin at the channel inlet.

The upstream boundary condition corresponds to a prescribed formative discharge per unit width q_{ua}^*, with the flow carrying a constant sediment flux per unit width in equilibrium with fluid flux q_{sua}^*. Following Copeland et al. (2000), the formative discharge is considered as a theoretical discharge that, maintained indefinitely, would produce the same morphological state as the natural long-term hydrograph.

At the channel mouth, the presence of the tides imposes an oscillation of the free surface H^*:

$$H^*|_{x^*=0} = a^* \sin(\omega^* t^*), \tag{3}$$

where a^* is the amplitude and $\omega^* = 2\pi/T^*$ the angular frequency of the tidal wave. Note that in the present work, we concentrate our attention on the dominant tidal constituent, neglecting the possible effect due to the presence of the different overtides such as MS_f (i.e., the fortnightly combination of the principal lunar and solar tidal constituent, Hoitink & Jay, 2016).

The one-dimensional equations governing the problem are the continuity and momentum balance equations for the fluid phase, coupled with the conservation of sediment mass. The problem is closed by the Engelund and Hansen (1967) relation for the total sediment discharge and by the Strickler relation for the friction coefficient (see Bolla Pittaluga, Tambroni, et al., 2015).

Taking advantage of the condition (2), a formal analytical perturbation solution for the long-term tidally averaged morphodynamic equilibrium of an estuary can be found with the assumption of small amplitude of the forcing tide at the channel inlet (i.e., no flow reversal is allowed at any cross section during the tidal cycle), expressed by the dimensionless parameter $\epsilon = a^*/D_{ua}^*$, and the further assumption of small values of the Froude number Fr_a (Seminara et al., 2012):

$$\epsilon = \frac{a^*}{D_{ua}^*} \ll 1, \qquad Fr_a = \frac{q_{ua}^*}{\sqrt{g^* D_{ua}^{*3}}} \sim \mathcal{O}(\epsilon), \tag{4}$$

with D_{ua}^* the uniform flow depth and g^* the gravitational acceleration. These assumptions are particularly appropriate in the case of wide, relatively shallow, micro-tidal estuaries (Seminara et al., 2001).

We refer to the paper of Seminara et al. (2012) for the details of the analysis, recalling that a synthesis can also be found in Bolla Pittaluga, Tambroni, et al. (2015). At the leading order problem one finds the steady uniform flow solution, being S_a, q_{ua}^*, and D_{ua}^* the river bed slope, the flow discharge per unit width, and its associated uniform flow depth, while the effect of residual terms deriving from tidal oscillations accounting for the river-tide interaction appears firstly in the solution at second order as a correction of the tidally averaged free surface elevation and flow depth.

The up to order ϵ^2 form of the tidally averaged longitudinal distribution of the flow depth $\langle D_a^* \rangle$, free surface elevation $\langle H_a^* \rangle$, and fluid and solid discharges $\langle q_a^* \rangle$ and $\langle q_{sa}^* \rangle$ for an estuary at equilibrium reads:

$$\langle D_a^*(x^*) \rangle = \underbrace{D_{ua}^*}_{\text{Zero -order term}} + \underbrace{\frac{a^{*2}}{D_{ua}^*} \mathcal{N}(\lambda_a) \exp\left(-2\mathrm{Re}(\mu_a) \frac{x^*}{D_{ua}^*} S_a\right)}_{\text{Second -order term,}} \tag{5a}$$

$$\langle H_a^*(x^*) \rangle = \underbrace{S_a x^*}_{\text{Zero -order term}} + \underbrace{\frac{a^{*2}}{D_{ua}^*} \mathcal{G}(\lambda_a) \left[\exp\left(-2\mathrm{Re}(\mu_a) \frac{x^*}{D_{ua}^*} S_a\right) - 1\right]}_{\text{Second -order term}}, \tag{5b}$$

$$\langle q_a^*(x^*) \rangle = q_{ua}^*, \tag{5c}$$

$$\langle q_{sa}^*(x^*) \rangle = q_{sua}^*, \tag{5d}$$

where

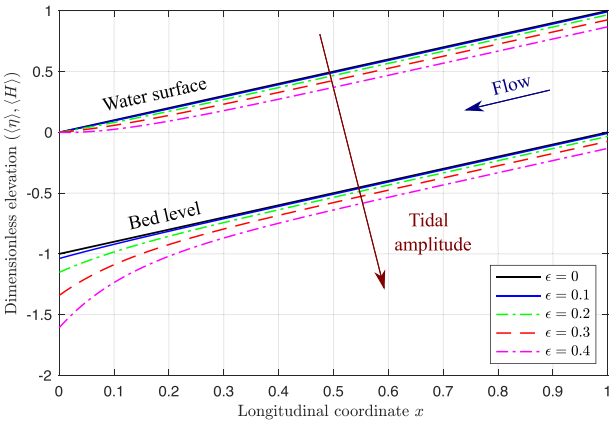

Figure 3. Longitudinal bed ($\langle\eta\rangle$) and free surface elevation profiles ($\langle H\rangle$) of an estuary at equilibrium, for increasing values of the tidal amplitude at the inlet. Dimensionless quantities are defined as follows: $(\langle\eta\rangle, \langle H\rangle) = (\langle\eta^*\rangle, \langle H^*\rangle)/D^*_{ua}$, $\epsilon = a^*/D^*_{ua}$, $x = x^* S_a/D^*_{ua}$.

$$\lambda_a = \frac{D^{*2}_{ua}\omega^*}{q^*_{ua}S_a}, \quad \mu_a = \frac{5}{3}\left[1 + \sqrt{1 + \frac{18}{25}i\lambda_a}\right], \tag{6a}$$

$$\mathcal{N}(\lambda_a) = \frac{13}{8} + \frac{5}{2}\frac{\mathrm{Im}(\mu_a)\lambda_a}{|\mu_a|^2} + \frac{10}{11}\frac{\lambda_a^2}{|\mu_a|^2}, \tag{6b}$$

$$\mathcal{G}(\lambda_a) = \frac{1}{2\mathrm{Re}(\mu_a)}\left[\frac{65}{36} + 5\frac{\lambda_a \mathrm{Im}(\mu_a)}{|\mu_a|^2} + \frac{167}{66}\frac{\lambda_a^2}{|\mu_a|^2}\right], \tag{6c}$$

with $i = \sqrt{-1}$ the imaginary unit, λ_a a dimensionless parameter measuring the effect of local inertia relative to convective transport in the longitudinal momentum equation, and the angle brackets denoting the tidal average of a generic function $\mathcal{F}$,

$$\langle\mathcal{F}\rangle = \frac{1}{T^*}\int_0^{T^*} \mathcal{F}\, dt^*. \tag{7}$$

Noteworthy, the second-order terms in (5a) and (5b) arise from the interaction of the $\mathcal{O}(1)$ and $\mathcal{O}(\epsilon)$ part of the solution. The latter, physically describing the propagation of a small-amplitude tidal wave on the fluvial stream, is characterized by a vanishing tidal average and thus does not appears explicitly in (5a) and (5b).

In Figure 3 we report the typical longitudinal bottom and the mean free surface equilibrium profiles of different estuaries with constant width and increasing values of tidal amplitude at the mouth. The effect of tidal oscillations exhibits itself with a steeper region at the mouth, which is the part of the channel dominated by tidal motion. Note that the slope in this region progressively increases as the tidal amplitude increases, becoming gradually characterized by the development of a concave down equilibrium profile. Finally, in the upper part, the estuary undergoes bed degradation as tidal amplitude increases.

2.2. Fluvial Bifurcations

The interaction between upstream and downstream control on fluvial bifurcations has been recently analyzed by Redolfi et al. (2019), who contextualized the concept of bifurcation stability in the framework of the morphodynamic influence theory of Zolezzi and Seminara (2001). We refer to the paper by Redolfi et al. (2019) for a review about the topic, and we limit ourselves to recalling the main results. A key role is played by the aspect ratio $\beta_a = W^*_a/(2D^*_a)$ of the upstream channel, depending on whether it falls above or below a threshold resonance value β_{res}, originally defined by Blondeaux and Seminara (1985). From the solution of the fully linear 2-D model, it was found that in the absence of external mechanisms, when $\beta_a < \beta_{res}$ the bifurcation is passive, and water and sediment are evenly partitioned downstream. But when β_a exceeds the resonance threshold, the formation of a steady bar in proximity of the node is triggered due to an instability mechanism, leading to an uneven distribution of water and sediment fluxes.

The one-dimensional model of Bolla Pittaluga et al. (2003) proved to capture the essential processes involved in these bifurcations dynamics. Two-dimensional effects are embodied by a physically based relation (*nodal point relation*): The last reach of the main channel is divided in two rectangular cells, αW^*_a long, which are able to laterally exchange sediment, depending on the value of the transverse bed slope.

In order to determine the solution (flow and bed topography), five nodal point conditions are required, namely, the mass and sediment conservation, the energy conservation along each cell, and the nodal point relation. The equilibrium diagram is characterized by a pitchfork bifurcation of the solution (Redolfi et al., 2019; Wiggins, 2003), where the point that either allows for multi-equilibrium states (β_{cr}) or discriminates between the sub-super critical character of the system can be evaluated through a linear stability analysis (Bolla Pittaluga, Coco, & Kleinhans, 2015) (for an example of the equilibrium diagram, see Redolfi et al., 2019, their Figure 4). The value of β_{cr} is equivalent to β_{res} once the parameter α is properly calibrated for each set of given parameters, in particular, the inlet Shields parameter θ_a and the dimensionless Chézy coefficient C_a.

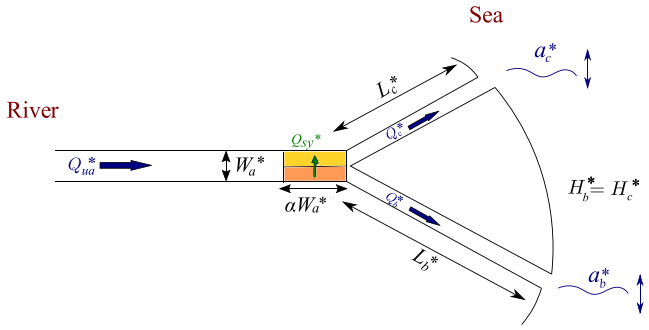

Figure 4. Scheme of the tidal bifurcation, with notation, adopted in the mathematical formulation: plan view.

The above bifurcation stability criterion has been successively tested against data on fluvial gravel bed and sand bed channels under the assumption of dominant bed load sediment transport (Bolla Pittaluga, Coco, & Kleinhans, 2015; Redolfi et al., 2019). However, in the case of bifurcations subject to a tidal forcing, the problem still lacks a comprehensive theoretical framework. Only recently, some works have addressed the problem of subtidal water division in a pure hydrodynamic fashion (Alebregtse & de Swart, 2016; Zhang et al., 2012).

3. Formulation of the Problem

Let us consider the tidal bifurcation sketched in Figure 4, consisting of an upstream channel a, splitting in two branches b and c, both debouching into the sea. The bed of the channels is assumed to be cohesionless, with uniform grain size d_s^* and relative density $s = \rho_s^*/\rho^*$, ρ^* and ρ_s^* being the density of water and sediment, respectively. The banks are frictionless and fixed, assuming the much slower character of the planimetric changes with respect to that associated with bed evolution. In this formulation, we consider channels with rectangular cross sections, neglecting the spatial variation of width associated with channel convergence. If this assumption is fairly reasonable in the upstream part of tidal deltas, it falls for reaches in the seaward part (Sassi et al., 2012). However, considering prismatic channels, as a first approach to the problem, allows us to investigate the effect of tidal propagation on the stability of a river bifurcation, separating the effect of channel convergence. A movable river bed with a constant width cross section throughout its length can exists when an artificial diversion is performed, with banks strengthened to prevent lateral erosion. Moreover, we neglect the possible effect of wind-waves and long-shore transport (Nienhuis et al., 2015) or the role of salinity stratification.

For the sake of simplicity, hereafter, the width of channel a is assumed to be twice the width of b and c ($W_a^* = 2W_{b,c}^*$). According with the two-cell scheme of Bolla Pittaluga et al. (2003), in proximity of the bifurcation node we consider two cells of length αW_a^*, which are feed uniformly by the incoming water and sediment fluxes.

The upstream channel a is supplied by a constant water discharge per unit width q_{ua}^* and by a constant sediment flux per unit width q_{sua}^* in equilibrium with q_{ua}^*. In general, the lengths of the two downstream branches b and c may be different; hence, the position of the node is set provided the distances L_b^* and L_c^* of the bifurcation from the sea in the branches b and c (see Figure 4) are given.

At the channels mouth we impose periodic oscillations of the free surface associated with a semi-diurnal M_2 tide ($T^* \simeq 12.4$ hr):

$$H_i^*|_{x^*=0} = a_i^* \sin(\omega^* t^*), \tag{8}$$

where a_i^*, with $i = \{b,c\}$, is the amplitude of tidal forcing (Equation 3) at the channels inlet.

The governing equations of the problem can be made dimensionless, once the variables are scaled as follows:

$$L_i^* = \frac{D_{ua}^*}{S_a} L_i, \quad t^* = \omega^{*-1} t, \quad (H_i^*, D_i^*, \eta_i^*) = D_{ua}^* (H_i, D_i, \eta_i), \tag{9a}$$

$$q_i^* = q_{ua}^* q_i, \quad q_{si}^* = q_{sua}^* q_{si}. \tag{9b}$$

Under the assumption of small tidal oscillations at the seaward boundary assumed here, no flow reversal is anywhere allowed in the system and the node does not change its flow characteristics during the tidal cycle (i.e., it never turns into a confluence during the ebb phase). Hence, following Bolla Pittaluga et al. (2003) we may impose the following nodal point conditions at the bifurcation:

$$\langle q_{bN} \rangle + \langle q_{cN} \rangle = \langle q_{aN} \rangle, \tag{10a}$$

$$\langle q_{sbN} \rangle + \langle q_{scN} \rangle = \langle q_{saN} \rangle, \tag{10b}$$

$$\langle q_{sbN}\rangle = \langle q_{bN}\rangle - \frac{2\alpha r}{\beta_a\sqrt{\theta_a}}\left(\langle \eta_{bN}\rangle - \langle \eta_{cN}\rangle\right), \tag{10c}$$

$$\langle H_{bN}\rangle = \langle H_{cN}\rangle = \langle H_{aN}\rangle, \tag{10d}$$

where the subscripts a,b,c refer to the branch of the bifurcation and the subscript N indicates the value of variables at the node.

The first two equations are representative of the water mass and sediment mass conservation. The third equation is the nodal point relation, and the last relationship consists in the constancy of water level.

Some parameters appear in (10c): r is a dimensionless constant tied with the intensity of gravitational contribution (Ikeda et al., 1981), and α is an empirical coefficient representative of the length where the effect of the bifurcation is felt which needs to be calibrated. Finally, θ_a is the value of the Shields parameter associated with the uniform flow in the channel a:

$$\theta_a = \frac{q_{ua}^{*2}}{(s-1)g^* d_s^* C_a^2 D_{ua}^{*2}}, \tag{11}$$

where C_a is the local value of the Chézy coefficient. Moreover, we employ the Engelund and Hansen (1967) predictor for the total sediment discharge per unit width:

$$q_{sua}^* = 0.05\, C_a^2 \theta_a^{2.5}\sqrt{(s-1)g^* d_s^{*3}}, \tag{12}$$

where C_a can be expressed through the classical Strickler relationship $C_a = k_s^* D_{ua}^{*1/6}/\sqrt{g^*}$, with k_s^* the Gauckler-Strickler coefficient.

Due to the unsteadiness of the flow, conditions (10a)–(10d) should be strictly imposed instantaneously, at any time of the tidal cycle. However, in analogy with the equilibrium definition of an estuary, and to a first approximation, a weaker form of equilibrium for the bifurcation may be achieved by imposing that bifurcation properties do not experience any net variation in a tidal cycle. This assumption allows to average the instantaneous nodal conditions in a tidal cycle to obtain (10a)–(10d).

Taking advantage of (10d) and noting that $H = \eta + D$, (10c) may be rewritten as

$$\langle q_{sbN}\rangle = \langle q_{bN}\rangle - \frac{2\alpha r}{\beta_a\sqrt{\theta_a}}\left(\langle D_{cN}\rangle - \langle D_{bN}\rangle\right). \tag{13}$$

Values of $\langle D_{bN}\rangle$ and $\langle D_{cN}\rangle$ need now to be specified. Each branch of the bifurcation is thus supposed to be a part of an estuary, characterized by a constant width (W_i^*), infinitely upstream fed by water and sediment discharges ($\langle q_i^*\rangle$ and $\langle q_{si}^*\rangle$) and forced by tidal oscillations with amplitude a_i^* at the inlet, in its long-term morphodynamic equilibrium condition. Basically, we are neglecting the possible effects related to the presence of the bifurcation in the equilibrium configuration of the two downstream branches and simply study the stability of a bifurcation connecting branches of estuaries each one supposed to be in its long-term morphodynamic equilibrium configuration. This is a key assumption of our model, which allows to impose the nodal point conditions in the form of (10a)–(10d). The possible effects of wave transmission and reflection due to the presence of the junction are implicitly neglected.

We may thus adopt the analytical solution of Seminara et al. (2012) (5) and evaluate at the node, along each branch, the following relationships for the dimensionless flow depth $\langle D(L)\rangle$, free surface elevation $\langle H(L)\rangle$, and both fluid and solid discharges $\langle q(L)\rangle$ and $\langle q_s(L)\rangle$, respectively (see Equation 5):

$$\langle D_i(L_i)\rangle = D_{ui} + \frac{\epsilon_i^2}{D_{ui}}\mathcal{N}(\lambda_i)\exp\left[-2\mathrm{Re}(\mu_i)q_{ui}^2 D_{ui}^{-13/3}L_i\right], \tag{14a}$$

$$\langle H_i(L_i)\rangle = L_i q_{ui}^2 D_{ui}^{-10/3} + \frac{\epsilon_i^2}{D_{ui}}\mathcal{G}(\lambda_i)\left[\exp\left(-2\mathrm{Re}(\mu_i)q_{ui}^2 D_{ui}^{-13/3}L_i\right) - 1\right], \tag{14b}$$

$$\langle q_i(L_i)\rangle = q_{ui}, \tag{14c}$$

$$\langle q_{si}(L_i)\rangle = q_{sui}, \tag{14d}$$

with $\mu(\lambda_i)$, $\mathcal{N}(\lambda_i)$, and $\mathcal{G}(\lambda_i)$ functions given by (6). Note that, as discharge partition at the bifurcation is not a priori known, variables have been made dimensionless according to relations (9) and, hence, in (14) the dimensionless parameters λ_a and $\epsilon_i = a_i^*/D_{ua}^*$, relative to the flow in the upstream channel a, arise.

The position of the bifurcation is set by the lengths L_b^* and L_c^* of the two branches; thus, the values of the variables appearing in (10a)–(10d) can be evaluated as

$$\langle q_{aN}\rangle = q_{ua}, \ \langle q_{saN}\rangle = q_{sua}, \tag{15a}$$

$$\langle q_{bN}\rangle = q_{ub}, \ \langle q_{sbN}\rangle = q_{sub}, \tag{15b}$$

$$\langle q_{cN}\rangle = q_{uc}, \ \langle q_{scN}\rangle = q_{suc}, \tag{15c}$$

$$\langle H_{bN}\rangle = \langle H_b(L_b)\rangle, \ \langle H_{cN}\rangle = \langle H_c(L_c)\rangle, \tag{15d}$$

$$\langle D_{bN}\rangle = \langle D_b(L_b)\rangle, \ \langle D_{cN}\rangle = \langle D_c(L_c)\rangle. \tag{15e}$$

Moreover having employed the Engelund and Hansen (1967) predictor for the solid discharge and the Strickler relation for the friction coefficient, the solid discharge per unit width q_{sui} in equilibrium with the fluid discharge per unit width q_{ui} must satisfy the following relationship:

$$q_{sui} = q_{ui}^5 D_{ui}^{-11/2}, \tag{16}$$

where for sake of simplicity, we set a constant value of the Strickler coefficient for the three branches.

At the end the problem can thus be expressed through the following algebraic nonlinear system in the unknown variables (q_{ub},q_{uc},D_{ub},D_{uc},$\langle D_{bN}\rangle$,$\langle D_{cN}\rangle$):

$$q_{ub} + q_{uc} = q_{ua}, \tag{17a}$$

$$q_{ub}^5 D_{ub}^{-11/2} + q_{uc}^5 D_{uc}^{-11/2} = q_{sua}, \tag{17b}$$

$$q_{ub}^5 D_{ub}^{-11/2} = q_{ub} - \frac{2\alpha r}{\beta_a\sqrt{\theta_a}}\left(\langle D_{cN}\rangle - \langle D_{bN}\rangle\right), \tag{17c}$$

$$\langle D_{bN}\rangle = D_{ub} + \frac{\epsilon_b^2}{D_{ub}}\mathcal{N}(\lambda_b)\exp\left[-2\mathrm{Re}(\mu_b)q_{ub}^2 D_{ub}^{-13/3}L_b\right], \tag{17d}$$

$$\langle D_{cN}\rangle = D_{uc} + \frac{\epsilon_c^2}{D_{uc}}\mathcal{N}(\lambda_c)\exp\left[-2\mathrm{Re}(\mu_c)q_{uc}^2 D_{uc}^{-13/3}L_c\right], \tag{17e}$$

$$\begin{aligned} &L_b q_{ub}^2 D_{ub}^{-10/3} + \frac{\epsilon_b^2}{D_{ub}}\mathcal{G}(\lambda_b)\left[\exp\left(-2\mathrm{Re}(\mu_b)q_{ub}^2 D_{ub}^{-13/3}L_b\right) - 1\right] = \\ &L_c q_{uc}^2 D_{uc}^{-10/3} + \frac{\epsilon_c^2}{D_{uc}}\mathcal{G}(\lambda_c)\left[\exp\left(-2\mathrm{Re}(\mu_c)q_{uc}^2 D_{uc}^{-13/3}L_c\right) - 1\right]. \end{aligned} \tag{17f}$$

Note that differently from the model of Bolla Pittaluga et al. (2003), the water depth in the two bifurcates is not given by the single uniform flow relationship, but, due to the presence of the tidal motion, it has a correction, expressed by the term involving ϵ_i^2, depending on the uniform flow characteristics, on the relative tidal amplitude at the inlet, and on the position of the node with respect of the sea (i.e., the length of the channels). For $\epsilon_i = 0$, $\langle D_{bN}\rangle = D_{ub}$, and $\langle D_{cN}\rangle = D_{uc}$, the system becomes independent from the length of the channels and coincides with the solution of Bolla Pittaluga et al. (2003).

The problem is firstly tackled analytically by means of a linearization procedure of the governing system of Equations 17a–17f to understand the controlling parameters that govern the behavior of the bifurcation (section 4.1). We then build on the linear analysis for the equilibrium solution of the whole nonlinear system, which is solved by means of the Newton-Raphson method (section 4.2).

4. Results

4.1. Linear Solution

The linear solution is obtained performing a Taylor expansion around the basic state, namely, the uniform flow conditions in channel a and a symmetrical water and sediment discharge distribution in the branches b and c. Moreover, for sake of simplicity, we initially consider equal length of the branches b and c and the same tidal forcing amplitude at the two inlets; in other words, we set:

$$\epsilon_b = \epsilon_c = \epsilon, \qquad L_c = L_b = L. \tag{18}$$

We can expand each generic variable Z (in our problem $(q_{ui}, D_{ui}, \langle D_i \rangle)$) in terms of the small parameter δ, as follows:

$$Z = Z_0 + \delta Z_1 + \mathcal{O}(\delta^2), \quad \delta \ll 1. \tag{19}$$

It is easy to see that at the linear level, the first-order perturbations of depths and water discharges in the two downstream branches are antisymmetric, allowing us to solve the problem separately for the two branches. With reference to channel b, after some algebra, we obtain the following linear system for the unknowns q_{ub1} and D_{ub1}:

$$\begin{cases} \xi_{11} q_{ub1} + \xi_{12} D_{ub1} = 0, \\ \xi_{21} q_{ub1} + \xi_{22} D_{ub1} = 0, \end{cases} \tag{20}$$

with the coefficients ξ_{jk}, $\{j,k\} = \{1,2\}$ as defined in Appendix A1, where the interested reader may find a complete description of the linear stability analysis performed. System (20) admits for nontrivial solutions provided the determinant of the matrix of the coefficients vanishes. Imposing such a condition, one finds the following algebraic relation for the critical aspect ratio β_{cr}:

$$\beta_{cr} = \frac{\alpha r}{\sqrt{\theta_a}} \left[\frac{2L + \epsilon^2 \left(\frac{10}{3} \Delta_{11} L + \Delta_{21} + 2\Delta_{12} L \right) + \epsilon^4 (\Delta_{12}\Delta_{21} - \Delta_{11}\Delta_{22})}{\frac{7}{12} L - \epsilon^2 \left(\Delta_{22} + \frac{11}{8} \Delta_{21} \right)} \right], \tag{21}$$

where for the expression of coefficients Δ_{jk}, depending on the flow and boundary conditions parameters, we refer to (A32)–(A35) in Appendix A1. Note that in the limit cases $\epsilon \to 0$ (no tidal forcing) and $L \to \infty$ (bifurcation located infinitely upstream), we recover the same expression for the critical aspect ratio found by Bolla Pittaluga, Coco, and Kleinhans (2015) in the purely riverine context:

$$\beta_{cr} = \frac{24}{7} \frac{\alpha r}{\sqrt{\theta_a}}. \tag{22}$$

We fixed as reference value $r = 0.5$ (e.g., Talmon et al., 1995) and $\alpha = 4$ in analogy with the riverine case (Redolfi et al., 2016). However, the values attained by these two parameters are not insignificant, since they respectively govern the intensity of the topographic effects and the limit length of the reach at which topographic effects are felt by the bed morphology. This distance is in turn tied with the wavelength of the steady damped alternate bars arising due to the instability mechanism shown by Redolfi et al. (2016). We may expect that in the sand bed case, especially in presence of a strong contribution of sediment carried in suspension, the bifurcation needs more space than in the classical gravel bed case to trigger the damped pattern (Federici & Seminara, 2006; Tubino et al., 1999).

The value of the critical aspect ratio β_{cr}, provided by Equation 21, is plotted in Figure 5 as a function of Shields parameter θ_a, for different values of the tidal forcing ϵ (Figure 5a) and of the scaled length of downstream channels L (Figure 5b). The reader may again appreciate as, when the tide is absent and/or the bifurcation is far enough from the sea, such that the effects of the tide are not felt by the junction, the plotted lines correspond to the solution of Bolla Pittaluga, Coco, and Kleinhans (2015) in the purely fluvial case.

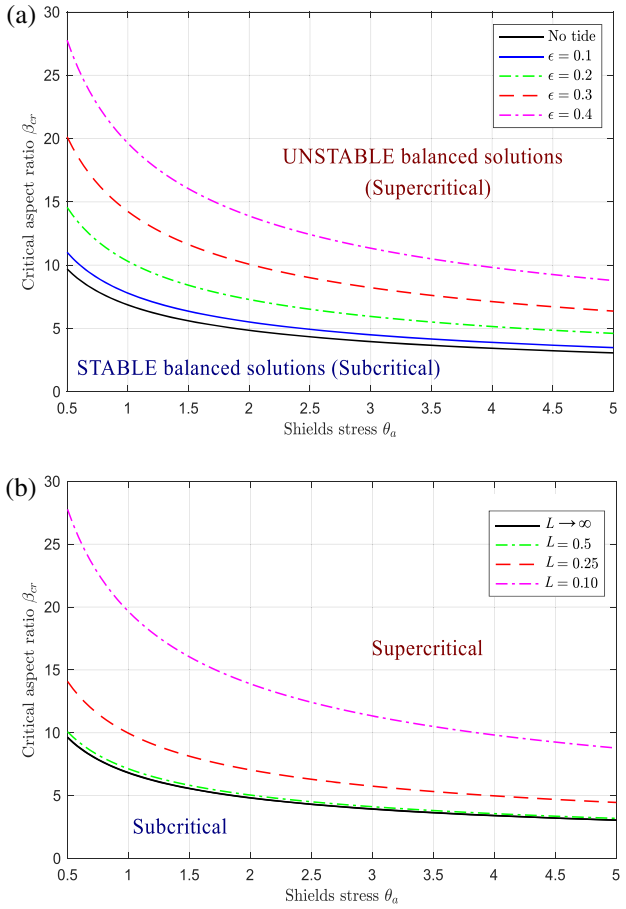

Figure 5. Neutral stability diagram as function of critical aspect ratio β_{cr} and Shields parameter θ_a for different values of (a) ϵ and (b) scaled position of the bifurcation node L. The solid black line is the solution in absence of tide of Bolla Pittaluga, Coco, and Kleinhans (2015). Input data: $\lambda_a = 10$, (a) $L = 0.1$, (b) $\epsilon = 0.4$.

Figure 5 shows a clear tendency: for a fixed value of θ_a, the value of critical aspect ratio which discriminates between the stable and unstable characters of the bifurcation grows as the bifurcation approaches the coast line and as the forcing tidal amplitude increases. The linear solution thus suggests that the effect of the tide is to stabilize the bifurcation. From a physical point of view, the presence of a tide hampers the triggering mechanisms which lead to destabilize the bifurcation.

The solution of Seminara et al. (2012) (Figure 3) provides useful information on a possible interpretation of the above results. Let us recall that the concept of bifurcation stability is strongly connected with the ability of the downstream branches to adapt their transport capacity to the incoming sediment input (Bolla Pittaluga, Coco, & Kleinhans, 2015). According to Seminara et al. (2012), the effect of the tide is to induce a progressive erosion wave that, proceeding landward from the channel mouth, migrates upstream along the estuary. Even just fairly small tidal amplitude is responsible for this erosive process observed theoretically (Bolla Pittaluga, Tambroni, et al., 2015; Seminara et al., 2012), experimentally (Finotello et al., 2019; Lentsch et al., 2018), in field-case study (Kästner et al., 2017; Leonardi et al., 2015; Shaw & Mohrig, 2014; Wagner & Mohrig, 2019), and with the utilization of process-based morphodynamic models (e.g., Delft3D) (Rossi et al., 2016), entailing an increase in transport capacity in each branch. As a consequence, provided the flow discharge partition at the bifurcation is the same, the tidal branches are deeper than their pure fluvial counterpart. We argue that this increase in flow depth along the tidal channels leads to a reduced dependency of the net sediment flux to a perturbation of the bed elevation.

Differently from the fluvial case, the critical conditions depend on the position of the node expressed by the variable L. Thus, Equation 21 may also be interpreted as to provide a critical distance L_{cr} for the stability of the bifurcation for a given value of β_a. We perform the above analysis in Figure 6 where we plot L_{cr} as a function of upstream aspect ratio β_a, for different values of ϵ and θ_a. The results suggest that shorter channels tend to be less asymmetric than longer channels similarly to what found by Salter et al. (2018), with the important difference that in their case the bifurcation dynamics is linked with the downstream sediment sinks, which lead to a possible different oscillation in water and sediment flux partitioning.

4.2. Nonlinear Solution

In the following we solve the fully nonlinear system (17a–17f), initially considering a symmetrical configuration set by (18). We successively relax this assumption, studying the implications of different boundary conditions like an unequal length of the two bifurcates or different values of tidal forcing at the inlets.

4.2.1. Symmetrical Downstream Branches and Tidal Forcing

The model solution can be expressed in terms of three dimensionless parameters relative to the flow conditions in the upstream channel, namely, the aspect ratio β_a, the Shields parameter θ_a (Equation 11), and parameter λ_a (Equation 6a).

In order to analyze the response of the bifurcation, we expressed the outputs in terms of discharge asymmetry index ΔQ (Bertoldi & Tubino, 2007; Redolfi et al., 2019):

$$\Delta Q = \frac{q^*_{ub} - q^*_{uc}}{2q^*_{ua}}, \tag{23}$$

with $\Delta Q = 0$ meaning a balanced partitioning of water fluxes, $\Delta Q = -1$ no flow in channel b, and $\Delta Q = +1$ no flow in channel c.

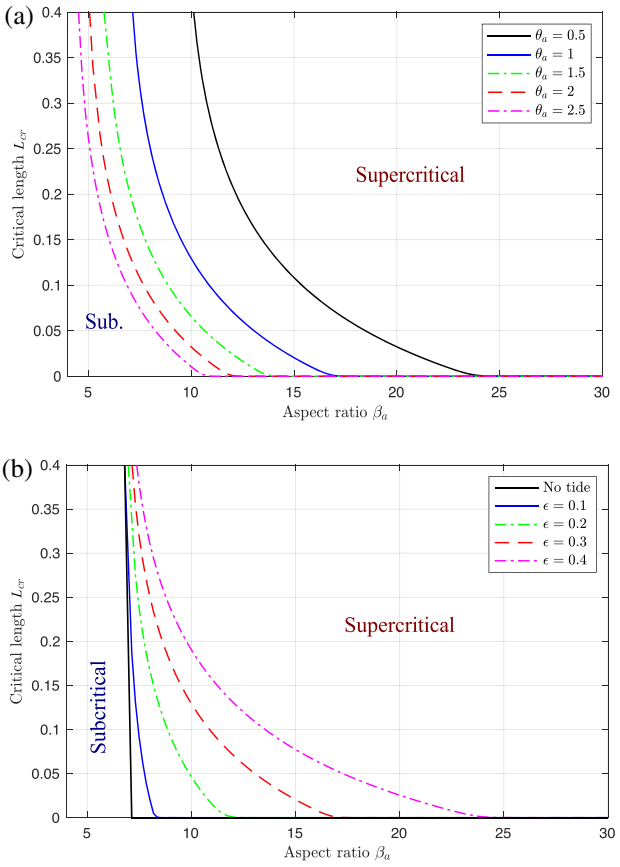

Figure 6. Neutral stability diagram as a function of critical length L_{cr} and upstream aspect ratio β_a, for (a) increasing values of Shields parameter θ_a and (b) tidal amplitude ϵ. The curves have an asymptote when the aspect ratio β_a tends to the critical value of the purely riverine case (Bolla Pittaluga, Coco, & Kleinhans, 2015). Input data: $\lambda_a = 10$, (a) $\epsilon = 0.3$, (b) $\theta_a = 1$.

In conformity with the approach adopted in section 4.1, when $\epsilon = 0$ or L is relatively high (for a given $\epsilon > 0$), the solution leads back to the bifurcation model of Bolla Pittaluga, Coco, and Kleinhans (2015) (Figure 7, black line): When the value of the aspect ratio β_a falls below a critical value β_{cr} (subcritical), the bifurcation keeps stable with an even partition of water and sediment; the latter situation becomes unstable when β_a exceeds the critical value (supercritical), leading to an unbalanced stable solution with one of the bifurcates carrying the larger fraction of the incoming water and sediment.

The solutions of the nonlinear system are also shown for (a) increasing values of the tidal forcing ϵ, keeping fixed the length of the downstream channels (Figure 7a), and (b) shortening the distance of the node from the sea, keeping fixed the amplitude of the tidal forcing ϵ (Figure 7b). The equilibrium solution still resembles the form of a pitchfork bifurcation with a threshold value of β_a distinguishing between a symmetrical or asymmetrical configuration; however, in agreement with the results found in the linear analysis, the value of the threshold β_{cr} at which the system evolves toward unbalanced equilibrium states increases, suggesting the tendency of the system to attain a more stable and balanced configuration for shorter channels (lower values of L) and/or greater tidal amplitudes.

We have to keep in mind that in this analysis we have discussed the stability of the bifurcation in terms of aspect ratio β_a (β_{cr}) as a function of ϵ and L, for given values of the Shields parameter θ_a and λ_a. This latter parameter is tied with the tidal motion (see systems 17a–17f). In particular, increasing values of λ_a induce an increase of critical aspect ratio β_{cr}, for fixed values of all the other parameters (θ_a, ϵ, L).

4.2.2. Asymmetrical Downstream Branches and Tidal Forcing

The former ideal configuration with symmetrical boundary conditions rarely takes place in natural environments. The presence of a meander bend in the upstream channel could feed non-uniformly the bifurcation node and favor the downstream channel at the outer bend (Kleinhans et al., 2008; Sassi et al., 2011). Moreover, the downstream channels may have different aggradation and progradation rates (Salter et al., 2018), different lengths (Kästner & Hoitink, 2019; Wagner & Mohrig, 2019), or asymmetric tidal forcing at the mouths. In this work we focus on the two latter conditions.

The importance of the sub-supercritical character of the bifurcation in the determination of the equilibrium configuration further emerges as a key factor when different downstream boundary conditions are applied in the two bifurcates. For example, if the two downstream channels have different lengths (e.g., $L_b < L_c$) and the same fixed value of ϵ, as illustrated in Figure 8a, when $\beta_a < \beta_{cr}$, more water flows toward the shorter channel ($\Delta Q > 0$). Moreover, the magnitude of the discharge asymmetry increases with the value of the upstream channel aspect ratio. The situation radically changes when β_a exceeds the threshold value. In this case, the equilibrium diagram mutates its topology, with the possibility for the system to attain new equilibrium states, in which most of the water discharge is carried by the longer channel ($\Delta Q < 0$). These results are in agreement with the analysis of Redolfi et al. (2019), which analyze the interaction of several forcing effects on bifurcation equilibrium like curvature of the upstream channel and a slope advantage for one of the two bifurcates (see their Figure 8). Choosing a different channels length thus corresponds to imposing a gradient advantage that tends to steer water and sediment flows toward the shorter branch (Redolfi et al., 2019).

Increasing the forcing tide in one of the two downstream channels has a similar effect to decreasing the length of the same channel. This exercise is performed in Figure 8b. In this case we fix the same length of the downstream channels (L) and progressively increase the value of the forcing tide at the inlet b ($\epsilon_b > \epsilon_c$). The results suggest that the downstream channel forced by the higher tide tends to

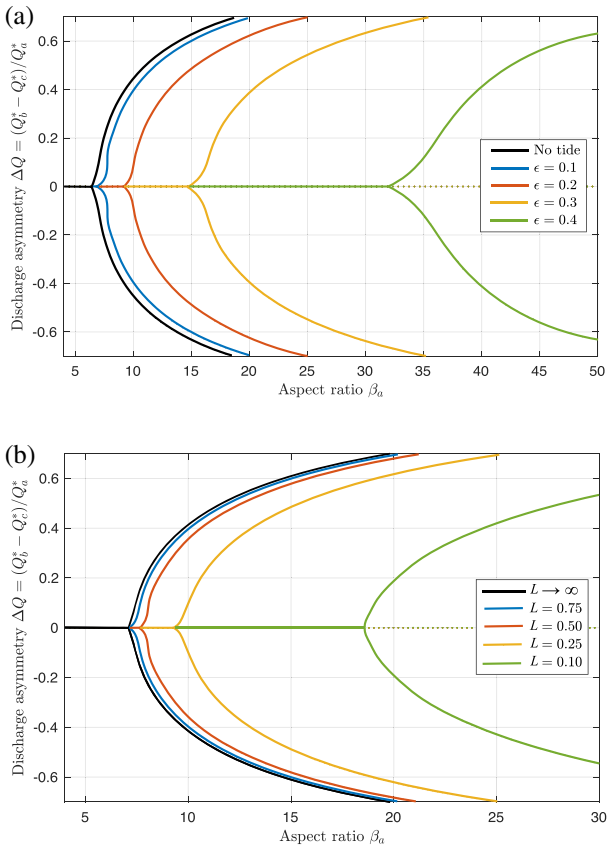

Figure 7. Equilibrium diagram for a tidal bifurcation with symmetrical downstream branch lengths for (a) different values of the tidal forcing ϵ and (b) scaled channel lengths L. Solid and dots lines denote stable and unstable solutions, respectively. Parameters are $\theta_a = 1$, $\lambda_a = 10$, (a) $L = 0.25$, (b) $\epsilon = 0.2$.

carry the most of water and sediment fluxes if $\beta_a < \beta_{cr}$. Vice versa, in the case $\beta_a > \beta_{cr}$, the possibility for the system to attain new different equilibrium states arises.

This behavior could be interpreted in the light of the aforementioned erosive character of tidal motion, which tends to deepen the channel subject to the higher tidal oscillations, in this way, favoring the allocation of water and sediment in that channel and enhancing the discharge inequality. The same effect has been outlined by the numerical simulations of Buschman et al. (2010) and Zhang et al. (2019).

5. Discussion

In the previous sections we have developed a one-dimensional model to analyze the equilibrium configurations and the stability of a simple channel bifurcation subject to a small monochromatic tidal oscillation. We have extended the previous models of Seminara et al. (2012), Bolla Pittaluga et al. (2003), and Bolla Pittaluga, Coco, and Kleinhans (2015) to account for the role of tides in determining bifurcation behavior, employing a local analysis and accounting for water depth variations in downstream channels due to tidal motion.

The linear analysis provides some insights on the controlling dimensionless parameters which govern the dynamics of the system under investigation. An important role is played by the forcing tidal amplitude and by the downstream channels length. Both increasing tides and channel shortening stabilize the bifurcation, resulting in a reduced maximum asymmetry in the supercritical case. The control exerted by this two parameters is not independent. The magnitude of the tidal effect is strongly correlated with the length of the branches (Figure 6). More precisely, the length of the branches modulates how the presence of a tidal fluctuation is felt by the upstream junction. Let us recall that the distance between the bifurcation and the open sea is scaled through a backwater length (i.e., the extent of channel impacted by nonuniform flow, Moodie et al., 2019), given by the ratio between the reference water depth D_{ua}^* and the channel slope S_a.

In order to substantiate our findings, we test the model with some literature data sets listed in Table S1 of the supporting information, comprehensive of bifurcations both found in natural deltas and modeled numerically. Note that we have included in our analysis also data from the Mossy Delta provided by Bolla Pittaluga, Coco, and Kleinhans (2015) representative of the purely riverine limit case (vanishing tidal forcing).

The results of the analysis are reported in Figure 9 in terms of a scaled aspect ratio $(\beta_a - \beta_{cr})/\beta_{cr}$, representing the relative distance from the critical conditions. For each bifurcation, Figure 9 includes estimates of the scaled aspect ratio both in the presence of tides (full markers) and for vanishing tides (empty markers). In particular, the latter configuration coincides with the purely fluvial case of Bolla Pittaluga, Coco, and Kleinhans (2015). From the analysis emerges that embodying the tidal effect brings to a reduced value of the scaled aspect ratio, and in turn, to a less unbalanced partition of water and sediment fluxes at the bifurcation. Physically, the results reported in Figure 9 suggest that tidal deltas have an improved capacity in maintaining open and morphodynamically active both downstream branches compared to their fluvial counterparts. This behavior differs from gravel bed braided rivers, which tend to concentrate their discharge and indeed their morphodynamic activity in few channels (Ashmore, 2001; Bertoldi & Tubino, 2007), or from river-dominated deltas, where the mouth-bar processes, which lead to shoreline progradation and shallower channels, increase the network complexity due repetitive avulsions (Jerolmack & Swenson, 2007; Olariu & Bhattacharya, 2006; Wright, 1977). Deltas under the influence of the tides show a minor number

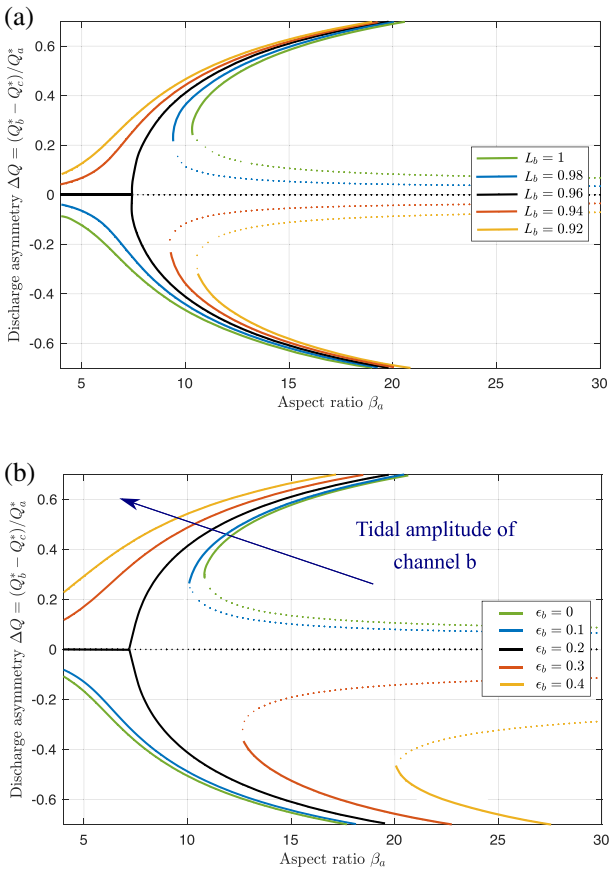

Figure 8. Equilibrium diagram in the case of different (a) downstream channels lengths and (b) tidal forcings. Length and tidal amplitude in channel *b* are changed, keeping constant the same parameters for channel *c*. Parameters are $\lambda_a = 10$, $\theta_a = 1$, (a) $\epsilon_b = \epsilon_c = 0.2$, $L_c = 0.96$, (b) $L_b = L_c = 1$, $\epsilon_c = 0.2$.

of active channels, with a more uniform distribution of discharge across channels, and a less frequent channel bifurcation and avulsion (Hoitink et al., 2017; Olariu & Bhattacharya, 2006; Rossi et al., 2016). As reported by Lentsch et al. (2018), the reduced mobility of distributaries emerges even for weak tides, and notably, when new accommodation space is created by rising sea level. The erosive character of the current which promotes channel deepening (Rossi et al., 2016) tends to hinder the development of a topographic gradient advantage due to backfilling (e.g., Hoyal & Sheets, 2009), mainly responsible for an avulsion event (Hoitink et al., 2020).

The deepening of the channels due to tides is captured by our model even in the fundamental assumptions made in section 3, which allow neglecting effects like the capture of tidal prism by one branch relative to the other as reported by Wagner and Mohrig (2019) or possible effects related to wave reflection at the bifurcation (e.g., Hill & Souza, 2006).

As previously stated, the response of the system analyzed in section 4.2 (Figures 7 and 8) strongly depends on the difference between the controlling parameters and their critical value. This is in agreement with the resonant criterion of Redolfi et al. (2016) and the laboratory observations of Bertoldi and Tubino (2007). In the case of strong inequalities in the discharge distribution and/or strong seasonal discharge fluctuations, such as in the Yangzte River Delta, this means that in the penalized reach the discharge amount from upstream river may be overwhelmed by the tidal currents, resulting in a reversing net flow in that channel during part of the tidal cycle. It is clear that such a case falls beyond the limit of validity of our model, which however is able to capture the development of the strong unbalances in discharge accommodation, observed in both a hydrodynamic semi-analytical model (Alebregtse & de Swart, 2016) and numerical simulations (e.g., Zhang et al., 2017, 2019).

Let us now discuss the main approximations our simple model relies on. Following a reductionist approach, in order to isolate the different effects, and to focus on those strictly related with the presence of tides, as a first approximation, we have neglected the spatial variation of channels geometry characterized by progressive seaward width increase, a distinct feature typical of tidal networks (e.g., Kästner et al., 2017; Lanzoni & D'Alpaos, 2015). As the analytical solution provided by Seminara et al. (2012) has already been formulated in this more general case, introducing width variations within the branches of the estuary is not a difficult task. The only difference is that the algebraic system (17a–17f) turns out to include a sequence of ordinary differential equations. A second main hypothesis concerns the uniformity of grain size and sediment transport closure. We have assumed a single value of the Strickler coefficient, related to a uniform bed material composition. As observed in the field works of Kästner et al. (2017) and Sassi et al. (2012), if a clear scaling in the geometric properties can be observed from upstream to downstream along the delta, which typically allows to separate the river-dominated to the tidal-dominated part of the delta, there is a clear difference in bed material composition between the branches that do not resemble the geometric scaling. This especially occurs among the main water course and the side distributaries. Grain sorting could have thus a strong influence in sediment division (Frings & Kleinhans, 2008; Kästner & Hoitink, 2019). Moreover, despite that our formulation relies on the Engelund and Hansen (1967) formula, which accounts for the total sediment flux, a deeper investigation on the role of suspended load is needed. Indeed, in the kind of environments under investigation, suspended sediment transport is dominant with a direct implication in the gravitational term in the nodal point relation, which probably would be weaker, thus increasing the probability of development of unbalanced bifurcations (Ikeda, 1989; Kleinhans et al., 2006). The employment of the Engelund and Hansen (1967) formula is strictly linked with the assumption of the cohesionless sediment character. However, in coastal settings, typically the presence of fine cohesive sediments is the rule rather than the

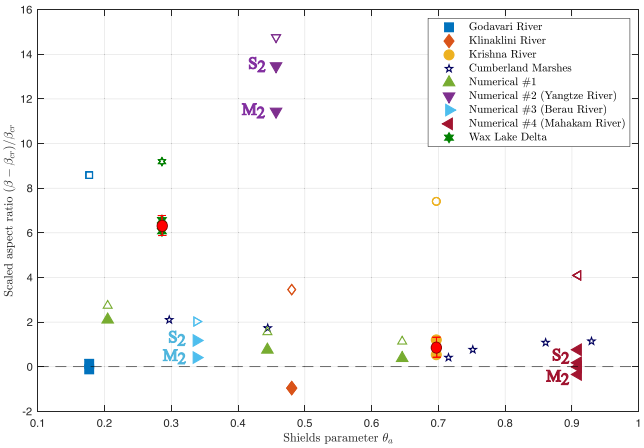

Figure 9. Estimated values of the scaled aspect ratio $(\beta_a - \beta_{cr})/\beta_{cr}$ as a function of Shields parameter θ_a for different natural and numerical tidal deltas. The dashed line denotes the theoretical threshold between the subcritical and supercritical regions. Geometrical markers represent different literature data, with empty markers referring to the values obtained from the purely riverine model (vanishing tides). Round red markers represent the median values of the analysis for the natural cases where the length of the branches has been estimated from satellite images. With M_2 and S_2 are denoted the principal lunar and solar tidal constituents, respectively. The full data sets along with the method adopted for the analysis are reported in the supporting information to this article.

exception, with a relevant implication for the morphodynamics of the system. The role of cohesion can be integrated relying upon a classical Partheniades-Krone description (e.g., Pritchard & Hogg, 2003; Toffolon & Lanzoni, 2010).

Moreover, our model results rely on the calibration of parameter α. This problem has been overpassed by Redolfi et al. (2016) for the pure fluvial case in the framework of morphodynamic influence by Zolezzi and Seminara (2001). A proper extension of the model of Redolfi et al. (2016) to account for the effect of tides and for both the role of bed load and suspended sediment transport would be necessary to complete the analysis. As suggested by Miori et al. (2012), it is reasonable to suppose that in sand bed river conditions, the flow structures induced by the bifurcation may extend further upstream than in the gravel bed case, having a greater influence on water flux partitioning.

Albeit simplistic, the symmetrical geometric configuration analyzed, which does not take into account the role of the bifurcation angle, is fully consistent with the present state-of-art modeling of river bifurcations. More specifically, Redolfi et al. (2016) show that relatively small junction angles (roughly less than 30°) do not affect the discharge partition, consistently with the laboratory experiments of Bertoldi and Tubino (2007) and the numerical simulations of Siviglia et al. (2013). This might not be the case in presence of a diversion or when the angle is significantly high as highlighted by Szewczyk et al. (2020). In these cases the bifurcation angle significantly controls channel abandonment, and the resulting channel fills when bed load is the main transport mechanism. In addition, from a recent work of Coffey and Shaw (2017) on a series of bifurcations in natural deltas and in an experimental delta, a mean characteristic angle around 70° emerges from all the measured cases. These results remark the necessity of a future investigation on the role of this often overlooked factor in bifurcation modeling.

Despite including the effect of the angle may be a difficult task, other important factors can be eventually included in the present formulation like the presence of a meander bend in the upstream channel (Kleinhans et al., 2008), a different phase of the tides at the mouth of the distributaries, or bifurcation width adjustment (removing the hypothesis of fixed banks) (Miori et al., 2006). In particular, the latter factor may be relevant in presence of relatively fast bank retreat phenomena as reported in different natural deltas (Hoitink et al., 2020).

Finally, the boundary conditions of the model rely on the steady character of fluvial and on the periodic character of the tidal forcing. These quantities are not steady. The extension to the unsteady problem would thus require a statistical formulation which is beyond the scope of this work.

6. Conclusions

The present work represents a first attempt to model the morphodynamic equilibrium of a river bifurcation subject to both a steady fluvial and a periodic tidal forcing. The theoretical framework stems from the one-dimensional two-cell model originally developed in the river case by Bolla Pittaluga et al. (2003), with the novel feature of accounting for the tidal effects through the employment of the tidally averaged, long-term equilibrium solution for estuaries proposed by Seminara et al. (2012).

The amplitude of the tidal oscillations and the bifurcation position with respect to the sea emerge as two key parameters affecting the possible equilibrium states of the system and its stability. The balanced or unbalanced character of the bifurcation depends on whether the width-to-depth ratio in the upstream channel falls below or above a critical value. This result is in analogy with the consolidated literature dealing with river bifurcations (in the absence of tides) and corroborates the important role of downstream boundary conditions on the process under investigation.

The model does not claim to describe in detail the property of flow field and bed topography in tidal bifurcations, and despite the simplifications that are introduced, it seems to capture some of the main features observed in both natural and numerically simulated micro-tidal deltas, providing a sound interpretation of one of the mechanisms linked with the stabilizing effect exerted by tides. For a major substantial validation of the model, there is the need of a systematic laboratory investigation on single bifurcations that, so far, has been successfully reproduced only for the pure fluvial case (e.g., Bertoldi & Tubino, 2007; Salter et al., 2019).

In this respect, the present model represents a suitable starting point for a number of interesting developments. First, as already discussed, a natural extension regards the planform shape of the distributaries. Second, it would be interesting to understand how bidirectional flows, peculiar in tide-dominated systems, may affect the morphodynamic equilibrium of the system as, in this case, the junction could switch its behavior from confluence to bifurcation, depending on the flood/ebb phase of the tide.

Appendix A: Linear Analysis

In this section we present the full linearization procedure, starting from system (10). As explained in the main text, for sake of symmetry we can study just one of the two branches.

Let us consider the continuity equation relative to channel b:

$$-1-2\alpha(q_{y0}+\delta\langle q_{y1}\rangle)+(1+\delta q_{ub1})=0, \tag{A1}$$

where the subscript 0 denotes the basic state and 1 the small perturbation term.

At the order $\mathcal{O}(\delta^0)$ we obtain $q_{y0}=0$, while at the first order $\mathcal{O}(\delta)$ one finds:

$$q_{ub1}=2\alpha\langle q_{y1}\rangle. \tag{A2}$$

The solution for the Exner equation and the nodal point relation is straightforward:

$$q_{sub1}=2\alpha\langle q_{sy1}\rangle, \tag{A3}$$

$$\langle q_{sy1}\rangle=\langle q_{y1}\rangle-\frac{r}{\beta_a\sqrt{\theta_a}}(\langle D_{c1}\rangle-\langle D_{b1}\rangle). \tag{A4}$$

Considering system (17) and expanding the parameter λ_i in powers of δ:

$$\lambda_i=\lambda_a\left[1+\frac{16}{3}\delta D_{ui1}\right][1-3\delta q_{ui1}], \tag{A5}$$

we get:

$$\lambda_i=\lambda_a+\delta\lambda_{i1},\ \ \lambda_{i1}=\lambda_a\left(\frac{16}{3}D_{ui1}-3q_{ui1}\right). \tag{A6}$$

In analogy the expansion of the coefficient μ_i reads:

$$\mu_i=\mu_a+\delta\mu_1\lambda_{i1}, \tag{A7}$$

where

$$\mu_a(\lambda_a)=\frac{5}{3}\left[1+\sqrt{1+\frac{18}{25}i\lambda_a}\right], \tag{A8}$$

$$\mu_1(\lambda_a)=\frac{3}{5}i\frac{1}{3\mu_a-1}. \tag{A9}$$

The expansion of the function $\mathcal{N}(\lambda_i)$ can be expressed in the form:

$$\mathcal{N}(\lambda_i) = \mathcal{N}_a + \delta\lambda_{i1}\mathcal{N}_1, \tag{A10}$$

with

$$\begin{aligned}\mathcal{N}_a(\lambda_a) &= \frac{13}{8} + \frac{5}{2}\frac{\lambda_a}{|\mu_a|^2}\left(\mathrm{Im}(\mu_a) + \frac{4}{11}\lambda_a\right),\\ \mathcal{N}_1(\lambda_a) &= \frac{5}{2}\frac{\lambda_a}{|\mu_a|^4}\left(\mathrm{Im}(\mu_a) + \frac{4}{11}\lambda_a\right)\left[|\mu_a|^2 - (\mu_1\mu_a + c.c.)\right] + \frac{5}{2}\frac{\lambda_a \mathrm{Im}(\mu_1)}{|\mu_a|^2},\end{aligned} \tag{A11}$$

with *c.c.* (or an overbar) standing for the complex conjugate of a complex number.

The exponential term can be expanded as follows:

$$\exp[-\mathscr{A}L] = (1 - \delta\mathscr{A}_{i1}L)\exp[-\mathscr{A}_a L], \tag{A12}$$

where we have denoted with $\mathscr{A}$ the following term:

$$\mathscr{A} = 2\mathrm{Re}(\mu_i) q_{ui}^2 D_{iu}^{-13/3}. \tag{A13}$$

Expansion of $\mathscr{A}$ gives:

$$\begin{aligned}\mathscr{A}_a(\lambda_a) &= 2\mathrm{Re}(\mu_a),\\ \mathscr{A}_{i1}(\lambda_a) &= \mathscr{A}_1^D D_{ui1} + \mathscr{A}_1^q q_{ui1},\end{aligned} \tag{A14}$$

where $\mathscr{A}_1^D$ and $\mathscr{A}_1^q$ are the following coefficients:

$$\mathscr{A}_1^D = -\frac{26}{3}\mathrm{Re}(\mu_a) + \frac{32}{3}\lambda_a \mathrm{Re}(\mu_1), \tag{A15}$$

$$\mathscr{A}_1^q = 4\mathrm{Re}(\mu_a) - 6\lambda_a \mathrm{Re}(\mu_1). \tag{A16}$$

We can finally write the term tied to the water depth affected by the tides in the two bifurcates in the linear form as follows:

$$\langle D_i \rangle = D_{iu} + \frac{\epsilon^2}{D_{iu}}\exp[-\mathscr{A}_i L], \tag{A17}$$

$$D_a = 1 + \epsilon^2 \mathcal{N}_a \exp[-2\mathrm{Re}(\mu_a)L], \tag{A18}$$

$$\langle D_{i1} \rangle = D_{ui1} + \epsilon^2 \exp(-\mathscr{A}_a L)[-D_{ui1}\mathcal{N}_a + \lambda_{i1}\mathcal{N}_1 - \mathcal{N}_a \mathscr{A}_{i1} L]. \tag{A19}$$

The last equation that we have to deal with is (17f):

$$\langle H_i(L) \rangle = L q_{ui}^2 D_{ui}^{-10/3} + \frac{\epsilon^2}{D_{iu}}\mathscr{G}(\lambda_i)[\exp(-\mathscr{A}_i L) - 1], \tag{A20}$$

$$H_a(L) = L + \epsilon^2 \mathscr{G}_a[\exp(-\mathscr{A}_a L) - 1], \tag{A21}$$

$$\begin{aligned}\langle H_{i1}(L) \rangle = L\left[2q_{ui1} - \frac{10}{3}D_{ui1}\right] + \epsilon^2\{(\mathscr{G}_1\lambda_{i1} - D_{ui1}\mathscr{G}_a)[\exp(-\mathscr{A}_a L) - 1] +\\ - L\mathscr{G}_a \mathscr{A}_{i1}\exp(-\mathscr{A}_a L)\}\end{aligned} \tag{A22}$$

Note that linearly:

$$\langle H_{i1}(L) \rangle = 0, \tag{A23}$$

hence,

$$-L\left[2q_{ui1}-\frac{10}{3}D_{ui1}\right]=\epsilon^2\{(\mathscr{G}_1\lambda_{i1}-D_{ui1}\mathscr{G}_a)[\exp(-\mathscr{A}_aL)-1]-L\mathscr{G}_a\mathscr{A}_{i1}\exp(-\mathscr{A}_aL)\}. \tag{A24}$$

Function $\mathscr{G}(\lambda_i)$ is derived as follows:

$$\mathscr{G}(\lambda_i)=\frac{1}{\mu_i+\mu_i}\left[\frac{65}{36}+5\frac{\lambda_i\mathrm{Im}(\mu_i)}{|\mu_i|^2}+\frac{167}{66}\frac{\lambda_i^2}{|\mu_i|^2}\right], \tag{A25}$$

$$\mathscr{G}_a(\lambda_a)=\frac{1}{2\mathrm{Re}(\mu_a)}\left[\frac{65}{36}+5\frac{\lambda_a\mathrm{Im}(\mu_a)}{|\mu_a|^2}+\frac{167}{66}\frac{\lambda_a^2}{|\mu_a|^2}\right], \tag{A26}$$

$$\begin{aligned}\mathscr{G}_1(\lambda_a,\lambda_{i1})=\frac{1}{\mu_a+\overline{\mu_a}}\Bigg[&-\mathscr{G}_a(\mu_1+\overline{\mu_1})+\frac{\lambda_{i1}}{|\mu_a|^2}\left(\frac{167}{33}\lambda_a+5\mathrm{Im}(\mu_a)+5\lambda_a\mathrm{Im}(\mu_1)\right)+\\&-\frac{\lambda_a}{|\mu_a|^4}\left(5\mathrm{Im}(\mu_a)+\frac{167}{66}\lambda_{i1}\lambda_a\right)(\mu_1\overline{\mu_a}+c.c.)\Bigg].\end{aligned} \tag{A27}$$

Finally, after some algebraic manipulations, the full linear system (20) can be obtained, where the coefficients ξ_{jk}, with $\{j,k\}=\{1,2\}$, are defined as follow:

$$\xi_{11}=4-\frac{4r\alpha}{\beta_a\sqrt{\theta_a}}\epsilon^2\Delta_{11}, \tag{A28}$$

$$\xi_{12}=-\frac{11}{2}-\frac{4r\alpha}{\beta_a\sqrt{\theta_a}}\{1+\epsilon^2\Delta_{12}\}, \tag{A29}$$

$$\xi_{21}=2L+\epsilon^2\Delta_{21}, \tag{A30}$$

$$\xi_{22}=-\frac{10}{3}L+\epsilon^2\Delta_{22}, \tag{A31}$$

and the coefficients Δ_{jk} read:

$$\Delta_{11}=\exp(-\mathscr{A}_aL)[-3\lambda_a\mathscr{N}_1-\mathscr{N}_a\mathscr{A}_1^qL], \tag{A32}$$

$$\Delta_{12}=\exp(-\mathscr{A}_aL)\left[-\mathscr{N}_a+\frac{16}{3}\lambda_a\mathscr{N}_1-\mathscr{N}_a\mathscr{A}_1^DL\right], \tag{A33}$$

$$\Delta_{21}=-3\mathscr{G}_1\lambda_a[\exp(-\mathscr{A}_aL)-1]-\mathscr{G}_a\exp(-\mathscr{A}_aL)\mathscr{A}_1^qL, \tag{A34}$$

$$\Delta_{22}=\left(\frac{16}{3}\mathscr{G}_1\lambda_a-\mathscr{G}_a\right)[\exp(-\mathscr{A}_aL)-1]-\mathscr{G}_a\exp(-\mathscr{A}_aL)\mathscr{A}_1^DL. \tag{A35}$$

Notation

0	parameter of the basic flow
1	first-order perturbation term
a	reference to the upstream channel
b,c	reference to the downstream channels
cr	critical conditions
N	value of a variable at the bifurcation
res	resonant conditions
u	uniform flow conditions
*	dimensional quantity
⟨ ⟩	tidally averaged quantity
Im()	imaginary part of a complex quantity
Re()	real part of a complex quantity

a^* [L]	tidal amplitude
$\mathscr{A}$ [-]	coefficients appearing in the linear analysis
C [-]	dimensionless Chézy coefficient
d_s^* [L]	sediment grain size
D^* [L]	flow depth
Fr [-]	Froude number
g^* [L] T^{-2}]	gravitational acceleration
$\mathscr{G}$ [-]	coefficient emerging from the Seminara et al. (2012) solution
H^* [L]	water surface elevation
k_s^* [$L^{1/3}$ T^{-1}]	Gauckler-Strickler coefficient
L^* [L]	downstream channels length
$\mathscr{N}$ [-]	coefficient emerging from the Seminara et al. (2012) solution
q^* [L]^2 T^{-1}]	flow discharge per unit width
q_s^* [L^2 T^{-1}]	sediment discharge per unit width
r [-]	dimensionless coefficient of Ikeda et al. (1981) formula
s [-]	relative density
S [-]	channel slope
t^* [T]	time
T^* [T]	tidal period
x^* [L]	longitudinal coordinate
W^* [L]	channel width
α [-]	dimensionless cells length of the upstream channel final reach
β [-]	half width-to-depth ratio (aspect ratio)
β_{cr} [-]	critical aspect ratio
β_{res} [-]	resonant aspect ratio
δ [-]	small parameter scaling the perturbation terms in the linearization
Δ [-]	coefficients of the linear bifurcation system
ΔQ [-]	discharge asymmetry index
ϵ [-]	dimensionless tidal amplitude scaled with the flow depth of the upstream channel
η^* [L]	bed elevation
θ [-]	Shields parameter
λ [-]	coefficient representing the effect of local inertia relative to convective transport in the momentum equation
μ [-]	coefficient appearing in the Seminara et al. (2012) model
ρ^* [M L^{-3}]	water density
ρ_s^* [M L^{-3}]	sediment density
ω^* [T^{-1}]	angular frequency of the tidal wave

Data Availability Statement

Matlab codes for the single estuary model and for the tidal bifurcation model are publicly available at the following site (https://zenodo.org/record/3784752#.XrAVQi-ubwd). The full data set along with an explanation of the methods adopted in the analysis of Figure 9 is reported in the supporting information to this article.

Acknowledgments
We thank the two anonymous reviewers, G. Salter, the editor, and the associate editor, whose careful and thoughtful reviews greatly enhanced the quality and readability of this article.

References

Alebregtse, N. C., & de Swart, H. E. (2016). Effect of river discharge and geometry on tides and net water transport in an estuarine network, an idealized model applied to the Yangtze Estuary. *Continental Shelf Research*, *123*, 29–49. https://doi.org/10.1016/j.csr.2016.03.028

Ashmore, P. (2001). Braiding phenomena: Statics and kinetics. In M. P. Mosley (Ed.), *Gravel bed rivers v* (pp. 95–121). Wellington, New Zealand: New Zealand Hydrological Society.

Bertoldi, W., & Tubino, M. (2007). River bifurcations: Experimental observations on equilibrium configurations. *Water Resources Research*, *43*, W10437. https://doi.org/10.1029/2007WR005907

Bertoldi, W., Zanoni, L., Miori, S., Repetto, R., & Tubino, M. (2009). Interaction between migrating bars and bifurcations in gravel bed rivers. *Water Resources Research*, *45*, W06418. https://doi.org/10.1029/2008WR007086

Blondeaux, P., & Seminara, G. (1985). A unified bar bend theory of river meanders. *Journal of Fluid Mechanics*, *157*, 449–470. https://doi.org/10.1017/S0022112085002440

Bolla Pittaluga, M., Coco, G., & Kleinhans, M. G. (2015). A unified framework for stability of channel bifurcations in gravel and sand fluvial systems. *Geophysical Research Letters*, *42*, 7521–7536. https://doi.org/10.1002/2015GL065175

Bolla Pittaluga, M., Repetto, R., & Tubino, M. (2003). Channel bifurcation in braided rivers: Equilibrium configurations and stability. *Water Resources Research*, *39*(3), 1–13. https://doi.org/10.1029/2003WR002754

Bolla Pittaluga, M., Tambroni, N., Canestrelli, A., Slingerland, R., Lanzoni, S., & Seminara, G. (2015). Where river and tide meet: The morphodynamic equilibrium of alluvial estuaries. *Journal of Geophysical Research: Earth Surface*, *120*, 75–94. https://doi.org/10.1002/2014JF003233

Buschman, F. A., Hoitink, A. J. F., Van Der Vegt, M., & Hoekstra, P. (2010). Subtidal flow division at a shallow tidal junction. *Water Resources Research*, *46*, W12515. https://doi.org/10.1029/2010WR009266

Coffey, T. S., & Shaw, J. B. (2017). Congruent bifurcation angles in river delta and tributary channel networks. *Geophysical Research Letters*, *44*, 11,427–11,436. https://doi.org/10.1002/2017GL074873

Copeland, R. R., Biedenharn, D. S., & Fischenich, J. C. (2000). Channel-forming discharge. *US Army Corps of Engineers, ERDC/CHL C* (December), 1–10.

Edmonds, D. A., & Slingerland, R. L. (2008). Stability of delta distributary networks and their bifurcations. *Water Resources Research*, *44*, W09426. https://doi.org/10.1029/2008WR006992

Engelund, F., & Hansen, E. (1967). A monograph on sediment transport in alluvial streams. Technical University of Denmark 0stervold-gade 10, Copenhagen K.

Federici, B., & Seminara, G. (2006). Effect of suspended load on sandbar instability. *Water Resources Research*, *42*, W07407. https://doi.org/10.1029/2005WR004399

Finotello, A., Lentsch, N., & Paola, C. (2019). Experimental delta evolution in tidal environments: Morphologic response to relative sea-level rise and net deposition. *Earth Surface Processes and Landforms*, *2015*, 2000–2015. https://doi.org/10.1002/esp.4627

Frings, R. M., & Kleinhans, M. G. (2008). Complex variations in sediment transport at three large river bifurcations during discharge waves in the river Rhine. *Sedimentology*, *55*(5), 1145–1171. https://doi.org/10.1111/j.1365-3091.2007.00940.x

Hackney, C. R., Darby, S. E., Parsons, D. R., Leyland, J., Best, J. L., Aalto, R., et al. (2020). River bank instability from unsustainable sand mining in the lower Mekong River. *Nature Sustainability*, *3*(3), 217–225. https://doi.org/10.1038/s41893-019-0455-3

Hiatt, M., & Passalacqua, P. (2015). Hydrological connectivity in river deltas: The first-order importance of channel-island exchange. *Water Resources Research*, *51*, 2264–2282. https://doi.org/10.1002/2014WR016149

Hill, A. E., & Souza, A. J. (2006). Tidal dynamics in channels: 2. Complex channel networks. *Journal of Geophysical Research*, *111*, C11021. https://doi.org/10.1029/2006JC003670

Hoitink, A. J. F., & Jay, D. A. (2016). Tidal river dynamics: Implications for deltas. *Reviews of Geophysics*, *54*, 240–272. https://doi.org/10.1002/2015RG000507

Hoitink, A. J. F., Nittrouer, J. A., Passalacqua, P., Shaw, J. B., Langendoen, E. J., Huismans, Y., & van Maren, D. S. (2020). Resilience of river deltas in the Anthropocene. *Journal of Geophysical Research: Earth Surface*, *125*, 1–24. https://doi.org/10.1029/2019JF005201

Hoitink, A. J. F., Wang, Z. B., Vermeulen, B., Huismans, Y., & Kästner, K. (2017). Tidal controls on river delta morphology. *Nature Geoscience*, *10*(9), 637–645. https://doi.org/10.1038/ngeo3000

Hoyal, D. C. J. D., & Sheets, B. A. (2009). Morphodynamic evolution of experimental cohesive deltas. *Journal of Geophysical Research*, *114*, F02009. https://doi.org/10.1029/2007JF000882

Ikeda, S. (1989). Sediment transport and sorting at bends, *River meandering* (Vol.12, pp. 103–125). Washington, DC: American Geophysical Union.

Ikeda, S., Parker, G., & Sawai, K. (1981). Bend theory of river meanders. Part 1. Linear development. *Journal of Fluid Mechanics*, *112*, 363–377. https://doi.org/10.1017/S0022112081000451

Iwantoro, A. P., Van DerVegt, M., & Kleinhans, M. G. (2019). Morphological evolution of bifurcations in tide-influenced deltas. *Earth Surface Dynamics Discuss*, *8*(2), 1–24.

Jerolmack, D. J., & Swenson, J. B. (2007). Scaling relationships and evolution of distributary networks on wave-influenced deltas. *Geophysical Research Letters*, *34*, L23402. https://doi.org/10.1029/2007GL031823

Kästner, K., & Hoitink, A. J. F. (2019). Flow and suspended sediment division at two highly asymmetric bifurcations in a river delta: Implications for channel stability. *Journal of Geophysical Research: Earth Surface*, *124*, 2358–2380. https://doi.org/10.1029/2018JF004994

Kästner, K., Hoitink, A. J. F., Vermeulen, B., Geertsema, T. J., & Ningsih, N. S. (2017). Distributary channels in the fluvial to tidal transition zone. *Journal of Geophysical Research: Earth Surface*, *122*, 696–710. https://doi.org/10.1002/2016JF004075

Kleinhans, M. G., Jagers, B., Mosselman, E., & Sloff, K. (2006). Effect of upstream meanders on bifurcation stability and sediment division in ID, 2D and 3D models. *Proceedings of the International Conference on Fluvial Hydraulics - River Flow 2006*, *2*, 1355–1362. https://doi.org/10.1201/9781439833865.ch144

Kleinhans, M. G., Jagers, H. R. A., Mosselman, E., & Sloff, C. J. (2008). Bifurcation dynamics and avulsion duration in meandering rivers by one-dimensional and three-dimensional models. *Water Resources Research*, *44*, W08454. https://doi.org/10.1029/2007WR005912

Kleinhans, M. G., Van Rosmalen, T. M., Roosendaal, C., & Van Der Vegt, M. (2014). Turning the tide: Mutually evasive ebb-and flood-dominant channels and bars in an experimental estuary. *Advances in Geosciences*, *39*, 21–26. https://doi.org/10.5194/adgeo-39-21-2014

Lanzoni, S., & D'Alpaos, A. (2015). On funneling of tidal channels. *Journal of Geophysical Research: Earth Surface*, *120*, 433–452. https://doi.org/10.1002/2014JF003203

Lanzoni, S., & Seminara, G. (2002). Long-term evolution and morphodynamic equilibrium of tidal channels. *Journal of Geophysical Research*, *107*(C1), 3001. https://doi.org/10.1029/2000JC000468

Lentsch, N., Finotello, A., & Paola, C. (2018). Reduction of deltaic channel mobility by tidal action under rising relative sea level. *Geology*, *46*(7), 599–602. https://doi.org/10.1130/G45087.1

Leonardi, N., Kolker, A. S., & Fagherazzi, S. (2015). Interplay between river discharge and tides in a delta distributary. *Advances in Water Resources*, *80*, 69–78. https://doi.org/10.1016/j.advwatres.2015.03.005

Leuven, J. R. F. W., Braat, L., van Dijk, W. M., de Haas, T., van Onselen, E. P., Ruessink, B. G., & Kleinhans, M. G. (2018). Growing forced bars determine nonideal estuary planform. *Journal of Geophysical Research: Earth Surface*, *123*, 2971–2992. https://doi.org/10.1029/2018JF004718

Miori, S., Hardy, R. J., & Lane, S. N. (2012). Topographic forcing of flow partition and flow structures at river bifurcations. *Earth Surface Processes and Landforms*, *37*(6), 666–679. https://doi.org/10.1002/esp.3204

Miori, S., Repetto, R., & Tubino, M. (2006). A one-dimensional model of bifurcations in gravel bed channels with erodible banks. *Water Resources Research*, *42*, W11413. https://doi.org/10.1029/2006WR004863

Moodie, A. J., Nittrouer, J. A., Ma, H., Carlson, B. N., Chadwick, A. J., Lamb, M. P., & Parker, G. (2019). Modeling deltaic lobe-building cycles and channel avulsions for the Yellow River Delta, China. *Journal of Geophysical Research: Earth Surface*, *124*, 2438–2462. https://doi.org/10.1029/2019JF005220

Nienhuis, J. H., Ashton, A. D., & Giosan, L. (2015). What makes a delta wave-dominated? *Geology*, *43*(6), 511–514. https://doi.org/10.1130/G36518.1

Olariu, C., & Bhattacharya, J. P. (2006). Terminal distributary channels and delta front architecture of river-dominated delta systems. *Journal of Sedimentary Research*, *76*, 212–233. https://doi.org/10.2110/jsr.2006.026

Paola, C., Twilley, R. R., Edmonds, D. A., Kim, W., Mohrig, D., Parker, G., et al. (2011). Natural processes in delta restoration: Application to the Mississippi Delta. *Annual Review of Marine Science*, *3*(1), 67–91. https://doi.org/10.1146/annurev-marine-120709-142856

Pritchard, D., & Hogg, A. J. (2003). Cross-shore sediment transport and the equilibrium morphology of mudflats under tidal currents. *Journal of Geophysical Research*, *108*(10), 11–1. https://doi.org/10.1029/2002jc001570

Redolfi, M., Zolezzi, G., & Tubino, M. (2016). Free instability of channel bifurcations and morphodynamic influence. *Journal of Fluid Mechanics*, *799*, 476–504. https://doi.org/10.1017/jfm.2016.389

Redolfi, M., Zolezzi, G., & Tubino, M. (2019). Free and forced morphodynamics of river bifurcations. *Earth Surface Processes and Landforms*, *44*(4), 973–987. https://doi.org/10.1002/esp.4561

Rossi, V. M., Kim, W., López, J. L., Edmonds, D., Geleynse, N., Olariu, C., et al. (2016). Impact of tidal currents on delta-channel deepening, stratigraphic architecture, and sediment bypass beyond the shoreline. *Geology*, *44*(11), 927–930. https://doi.org/10.1130/G38334.1

Salter, G., Paola, C., & Voller, V. R. (2018). Control of delta avulsion by downstream sediment sinks. *Journal of Geophysical Research: Earth Surface*, *123*, 142–166. https://doi.org/10.1002/2017JF004350

Salter, G., Voller, V. R., & Paola, C. (2019). How does the downstream boundary affect avulsion dynamics in a laboratory bifurcation? *Earth Surface Dynamics*, *7*, 911–927. https://doi.org/10.5194/esurf-2019-26

Sassi, M. G., Hoitink, A. J. F., De Brye, B., & Deleersnijder, E. (2012). Downstream hydraulic geometry of a tidally influenced river delta. *Journal of Geophysical Research*, *117*, F04022. https://doi.org/10.1029/2012JF002448

Sassi, M. G., Hoitink, A. J. F., De Brye, B., Vermeulen, B., & Deleersnijder, E. (2011). Tidal impact on the division of river discharge over distributary channels in the Mahakam Delta. *Ocean Dynamics*, *61*(12), 2211–2228. https://doi.org/10.1007/s10236-011-0473-9

Schuttelaars, H. M., & Swart, H. E. D. (2000). Multiple morphodynamic equilibria in tidal embayments. *Journal of Geophysical Research*, *105*, 105–118. https://doi.org/10.1029/2000JC900110

Seminara, G., Bolla Pittaluga, M., & Tambroni, N. (2012). Morphodynamic equilibrium of tidal channels. Environmental Fluid Mechanics: Memorial volume in honour of Prof. Gerhard H. Jirka, pp. 153-174, https://doi.org/10.1201/b12283

Seminara, G., Lanzoni, S., Bolla Pittaluga, M., & Solari, L. (2001). Estuarine patterns: An introduction to their morphology and mechanics. *Lecture Notes in Physics*, *582*, 455–499. https://doi.org/10.1007/3-540-45670-8_19

Seminara, G., Lanzoni, S., Tambroni, N., & Toffolon, M. (2010). How long are tidal channels? *Journal of Fluid Mechanics*, *643*, 479–494. https://doi.org/10.1017/S0022112009992308

Shaw, J. B., & Mohrig, D. (2014). The importance of erosion in distributary channel network growth, Wax Lake Delta, Louisiana. *Geological Society Of America*, *42*, 31–34. https://doi.org/10.1130/G34751.1

Siviglia, A., Stecca, G., Vanzo, D., Zolezzi, G., Toro, E. F., & Tubino, M. (2013). Numerical modelling of two-dimensional morphodynamics with applications to river bars and bifurcations. *Advances in Water Resources*, *52*, 243–260. https://doi.org/10.1016/j.advwatres.2012.11.010

Slingerland, R., & Smith, N. D. (2004). River avulsions and their deposits. *Annual Review of Earth and Planetary Sciences*, *32*(1), 257–285. https://doi.org/10.1146/annurev.earth.32.101802.120201

Szewczyk, L., Grimaud, J.-L., & Cojan, I. (2020). Experimental evidences for bifurcation angles control on abandoned channel fill geometry. *Earth Surface Dynamics*, *8*, 275–288. https://doi.org/10.5194/esurf-2019-79

Talmon, A. M., Struiksma, N., & Van Mierlo, M. C. L. M. (1995). Laboratory measurements of the direction of sediment transport on transverse alluvial-bed slopes. *Journal of Hydraulic Research*, *33*(4), 495–517. https://doi.org/10.1080/00221689509498657

Tambroni, N., Bolla Pittaluga, M., & Seminara, G. (2005). Laboratory observations of the morphodynamic evolution of tidal channels and tidal inlets. *Journal of Geophysical Research*, *110*, F04009. https://doi.org/10.1029/2004JF000243

Todeschini, I., Toffolon, M., & Tubino, M. (2008). Long-term morphological evolution of funnel-shape tide-dominated estuaries. *Journal of Geophysical Research*, *113*, C05005. https://doi.org/10.1029/2007JC004094

Toffolon, M., & Lanzoni, S. (2010). Morphological equilibrium of short channels dissecting the tidal flats of coastal lagoons. *Journal of Geophysical Research*, *115*, F04036. https://doi.org/10.1029/2010JF001673

Tubino, M., Repetto, R., & Zolezzi, G. (1999). Free bars in rivers. *Journal of Hydraulic Research*, *37*(6), 759–775. https://doi.org/10.1080/00221689909498510

Wagner, W., & Mohrig, D. (2019). Flow and sediment flux asymmetry in a branching channel delta. *Water Resources Research*, *55*, 9563–9577. https://doi.org/10.1029/2019WR026050

Wang, Z. B., De Vries, M., Fokkink, R. J., & Langerak, A. (1995). Stability of river bifurcations in 1D morphodynamic models. *Journal of Hydraulic Research*, *33*(6), 739–750. https://doi.org/10.1080/00221689509498549

Wiggins, S. (2003). *Introduction to applied nonlinear dynamical systems and chaos*. New York: Springer.

Wright, L. D. (1977). Sediment transport and deposition at river mouths: A synthesis. *Geological Society Of America Bulletin*, *88*(6), 857–868. https://doi.org/10.1130/0016-7606(1977)88<857:STADAR>2.0.CO;2

Xu, F., Coco, G., Tao, J., Zhou, Z., Zhang, C., Lanzoni, S., & D'Alpaos, A. (2019). On the morphodynamic equilibrium of a short tidal channel. *Journal of Geophysical Research: Earth Surface*, *124*, 639–665. https://doi.org/10.1029/2018JF004952

Zhang, W., Feng, H., Hoitink, A. J. F., Zhu, Y., Gong, F., & Zheng, J. (2017). Tidal impacts on the subtidal flow division at the main bifurcation in the Yangtze River Delta. *Estuarine, Coastal and Shelf Science*, *196*, 301–314. https://doi.org/10.1016/j.ecss.2017.07.008

Zhang, W., Feng, H., Zhu, Y., Zheng, J., & Hoitink, A. J. F. (2019). Subtidal flow reversal associated with sediment accretion in a delta channel. *Water Resources Research*, *55*, 10,781–10,795. https://doi.org/10.1029/2019WR025945

Zhang, E. F., Savenije, H. H. G., Chen, S. L., & Mao, X. H. (2012). An analytical solution for tidal propagation in the Yangtze Estuary, China. *Hydrology and Earth System Sciences*, *16*, 3327–3339. https://doi.org/10.5194/hess-16-3327-2012

Zhou, Z., Coco, G., Townend, I., Olabarrieta, M., van der Wegen, M., Zheng, G., et al. (2016). Is "morphodynamic equilibrium" an oxymoron? *Earth Science Reviews*, *165*, 157–167. https://doi.org/10.1016/j.earscirev.2016.12.002

Zolezzi, G., & Seminara, G. (2001). Downstream and upstream influence in river meandering. Part 1. General theory and application to overdeepening. *Journal of Fluid Mechanics*, *438*(July), 183–211. https://doi.org/10.1017/S0022112001004281